Accepted Manuscript

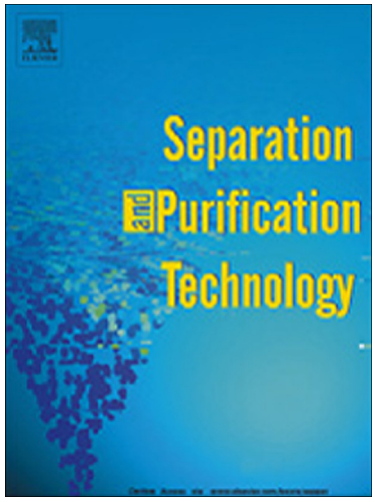

Enhanced Desalination via Functionalized Carbon Nanotube Immobilized Membrane in Direct Contact Membrane Distillation

Sagar Roy, Madhuleena Bhadra, Somenath Mitra

PII: S1383-5866(14)00498-5
DOI: http://dx.doi.org/10.1016/j.seppur.2014.08.009
Reference: SEPPUR 11930

To appear in: *Separation and Purification Technology*

Received Date: 21 February 2014
Revised Date: 1 August 2014
Accepted Date: 13 August 2014

Please cite this article as: S. Roy, M. Bhadra, S. Mitra, Enhanced Desalination via Functionalized Carbon Nanotube Immobilized Membrane in Direct Contact Membrane Distillation, *Separation and Purification Technology* (2014), doi: http://dx.doi.org/10.1016/j.seppur.2014.08.009

This is a PDF file of an unedited manuscript that has been accepted for publication. As a service to our customers we are providing this early version of the manuscript. The manuscript will undergo copyediting, typesetting, and review of the resulting proof before it is published in its final form. Please note that during the production process errors may be discovered which could affect the content, and all legal disclaimers that apply to the journal pertain.

ACCEPTED MANUSCRIPT

Enhanced Desalination via Functionalized Carbon Nanotube Immobilized Membrane in Direct Contact Membrane Distillation

Sagar Roy, Madhuleena Bhadra and Somenath Mitra*

Department of Chemistry and Environmental Science

New Jersey Institute of Technology

Newark, NJ, 07102

USA

* Corresponding Author

Somenath Mitra, 973-596-5611(t), 973-596-3586(F), mitra@njit.edu

ACCEPTED MANUSCRIPT

ACCEPTED MANUSCRIPT

Abstract

In this paper, for the first time we report the development of carbon nanotube immobilized membrane (CNIM) on porous polypropylene support for direct contact membrane distillation (DCMD) desalination application. We also describe the effect of specific interaction of functional group of carbon nanotubes (CNTs) with water moisture on the enhancement of water vapor flux in DCMD via alteration of polar-non polar nature of membrane surface. The incorporation of carboxylic acid (-COOH) functional group on carbon nanotubes alters the hydrophilic-hydrophobic interaction of water moistures with the membrane surface that provides additional pathway for enhanced water vapor transport. The water vapor flux was obtained 36.8 $kg/m^2.hr$ at 70^0C for CNT-COOH-PP, which is 51.5% higher than unmodified polypropylene membrane at salt concentration 10000 ppm in feed. The salt rejection was found greater than 99.9% at salt concentration 10000 ppm in feed solution. An increase in mass transfer coefficient about 1.5 times was also observed for CNT-COOH-PP membrane. The CNIM also exhibits higher thermal stability at elevated temperatures.

Key words:

Functionalized MWCNTs; Hydrophilic-hydrophobic interaction; Direct contact membrane distillation; Desalination; Mass transfer coefficient

ACCEPTED MANUSCRIPT

ACCEPTED MANUSCRIPT

1. Introduction

With increasing demand for fresh water, sea water desalination technology has been developing quickly in the past decades. Low energy consumption makes membrane based techniques such as reverse osmosis (RO) and membrane distillation (MD) attractive alternatives. Compared to thermal distillation, MD is a membrane based evaporation process where the driving force is the temperature-induced vapor pressure difference caused by having a hot feed and a cold permeate. Typically, MD is carried out at 60-90ºC, which is significantly lower than conventional distillation. Therefore, it has the potential to generate high quality drinking water using only low temperature heat sources such as waste heat from industrial processes and solar energy. The main effort in optimal design of MD systems is the maximization of solute rejection and flux, which would make MD commercially viable. A key component in such a process is the membrane itself because it determines both flux and selectivity.

The enhancement of membrane performances by developing novel membrane architecture is of great importance for MD. Several membrane materials based on polypropylene (PP), polyvinylidene difluoride (PVDF) and Teflon have been tested [1-2]. Variety of surface modification of MD membranes have been performed by radiation graft polymerization, plasma polymerization, grafting ceramic membranes, hydrophobic or hydrophilic surface coating, casting hydrophobic polymer over flat sheet or porous fibers as supports, co-extrusion spinning and use of surface modifying macromolecules (SMMs) [3-9]. A dual-layer hydrophilic–hydrophobic polyacrylonitrile (PAN)–PVDF hollow fiber membranes has been reported [10] along with the blending of hydrophilic base polymer with a hydrophobic surface modifying macromolecules [11]. More recent developments include surfaces modification with zeolite [12],

ACCEPTED MANUSCRIPT

clay nanocomposites nanofiber [13], silane grafting [14] and modification by hydrophobic porous alumina [15].

Carbon nanotube based membranes have been used in a variety of separation applications that range from pervaporation to nanofiltration [16-19]. The CNTs have been incorporated in the membranes by making polymer composites [18] and via chemical vapor deposition [20]. The combination of extremely high aspect ratio with small dimensions attracts them for molecular scale transport applications. Additionally, atomic scale smoothness and chemical inertness of the graphitic walls plays a critical role in the transport of water molecules [21]. Moreover, effective functionalization with controlled surface charges and hydrophilicity leads to improved fouling resistance and salt rejection [22, 23]. Synthesis of free-standing and silicon-chip supported vertically aligned CNTs membranes by a complex synthesis method have been reported for RO, and high permeability for such CNTs membranes has been confirmed [24]. At the same time self-supporting CNT Bucky-Paper membranes [25] as well as interfacially polymerized bucky-papers have also been used in MD.

Recently we have demonstrated different types of prefabricated CNT immobilized membranes, referred to as carbon nanotube immobilized membrane (CNIM) with varying degree of solute-membrane interactions, which is one of the major physicochemical factors affecting the permeability and selectivity. The CNTs on the membrane surface not only serve as a sorbent but also provide an additional pathway for solute transport. These membranes have been used in nanofiltration, solvent extraction and pervaporation, and have demonstrated superior performance [18, 26, 27]. We have already employed the CNIM successfully in sweeping gas membrane distillation (SGMD) to show significant enchantment in desalination [28]. It was observed that the water vapor flux for SGMD remained constant with increasing salt concentration, reaching

ACCEPTED MANUSCRIPT

up to 19.2 kg/m^2.hr. However, the SGMD configuration is relatively complex and higher condenser capacity is required to entrap the water vapors compared to direct contact membrane distillation (DCMD) where pure water is used in the permeate side as the condensing medium. The overall water vapor flux in SGMD was also reported lower compared to DCMD [29, 30]. The objective of this paper is to implement polypropylene CNIM in DCMD.

2. Experimental

2.1. Chemicals, materials and membrane modules

Sodium chloride (NaCl) was obtained from Sigma–Aldrich (St. Louis, MO) and deionized water (Barnstead 5023, Dubuque, Iowa) were used in all experiments. Flat polypropylene (PP) membrane (Celgard, LLC, Charlotte, NC) of 35 μm thickness, 0.045 μm pore size and 68% porosity were used in this DCMD experiments. DCMD test cell was fabricated from polytetrafluoroethylene (PTFE) material due to its high temperature stability.

The raw MWCNTs were purchased from Cheap Tubes Inc., Brattleboro, VT. The MWCNTs were further purified and functionalized with carboxylic (-COOH) groups in our laboratory [31]. The average diameters of the CNTs were ~30 nm and a length give range 15 μm.

2.2. Experimental procedure

The experimental set up for DCMD is illustrated in Fig. 1. The set up comprised PTFE membrane cell having an effective membrane area of 14.5 cm^2, Viton O-rings, PTFE tubing, PFA and PTFE connectors, feed and permeate flow pump (Cole Parmer, Vernon Hills, IL), circulating heated temperature bath (GP-200) and circulating chiller (MGW Lauda RM6).

ACCEPTED MANUSCRIPT

The hot aqueous NaCl solution of various concentrations was circulated on one side of the membrane in the DCMD cell. The temperature of the feed brine was maintained by using a temperature regulated hot oil bath. Cold distilled water was circulated on the other side of the membrane. Inlet and outlet temperatures of feed and permeate side was monitored by using a K-type temperature probe (Cole-parmer). Makeup water was added continuously to the feed side to maintain constant concentration throughout the experiment. The concentration of the feed brine and permeate were measured using a conductivity meter (Jenway, 4310). Each experiment was repeated at least three times to ensure reproducibility and relative standard deviation was found less than 1%.

2.2. Fabrication of f-CNT immobilized membrane

Effective dispersal of CNTs and immobilization on the membrane surfaces is considered an essential step in CNIM fabrication. 10 mg of CNTs was dispersed in acetone and sonicated for 3 hr. while 0.2 mg polyvinyledene difluoride (PVDF) was dissolved in acetone and mixed with CNTs dispersion. The mixture was then sonicated for another 30 minutes and used to fabricate the CNIM on porous PP.

The CNIM-PP membrane was characterized using scanning electron microscopy (SEM) (Leo 1530 VP, Carl Zeiss SMT AG Company, Oberkochen, Germany). Thermogravimetric analysis (TGA) was used to investigate the enhancement in thermal stability of modified membrane. TGA was carried out using a Perkin-Elmer Pyris 7 TGA system at a heating rate of 10°C/min in air. Confocal Raman imaging and Raman spectra were measured using a Thermo electron Nicolet Raman spectrometer.

ACCEPTED MANUSCRIPT

ACCEPTED MANUSCRIPT

2.3. Gas Permeation Tests

The effective surface porosity over the effective pore length was measured by gas permeation test as described in literature [32]. The total molar flux per unit trans membrane pressure difference across the porous PP membrane can be described as

$$\frac{J_i}{\Delta p} = \frac{2}{3}\left(\frac{8RT}{\pi M}\right)^{0.5}\frac{1}{RT}\frac{r\varepsilon}{L_p} + \frac{\bar{p}}{8\mu RT}\frac{r^2\varepsilon}{L_p} \quad (1)$$

where ε is surface porosity, r is mean pore radius of the membrane, is gas viscosity, R is gas constant, $\bar{p}$ is the average of feed and permeate side pressure, M is molecular weight of gas, L_p is effective pore length and T is temperature (K). The first term in this equation represents the contribution from Knudsen flow and the second term is due to Poiseuille flow. The gas permeation flux per unit driving force ($J_i/\Delta p$) can be calculated as from the following equation.

$$\frac{J_i}{\Delta P} = \frac{N_{t,i}}{A_t} \quad (2)$$

where, $N_{t,i}$ is total molar gas permeation rate (mol s^{-1}), ΔP is the trans membrane pressure difference across the membrane area A_t. The total gas permeation rate through the membrane at different pressures was measured using a soap bubble flow meter. From a plot of the nitrogen flux ($J_i/\Delta p$) against the mean gas pressure $\bar{p}$, the mean pore size (r) and the effective surface porosity over pore length, ε/L_p, can be obtained from the slope S_o and the intercept I_o as follows:

$$r = \frac{16}{3}\left(\frac{S_o}{I_o}\right)\left(\frac{8RT}{\pi M}\right)^{0.5}\mu_i \quad (3)$$

ACCEPTED MANUSCRIPT

$$\frac{\varepsilon}{L_p} = \frac{8\mu_i RTS_o}{r^2} \quad (4)$$

3. Results and discussion

3.1 Characterization of the Membranes

Effective porosity over pore length of the membrane was calculated from equation 4 and was obtained 2.4 X 10^{-5} m^{-1} for unmodified membrane. The value did not show any significant change for CNIM membranes as very small amount of CNTs has been used to fabricate the membrane.

Fig. 2a, b and c show the SEM images of the surface of the unmodified PP membrane, CNT-PP and CNT-COOH-PP membrane respectively. SEM image of CNT-PP showed a slight agglomeration of raw CNTs on the membrane surface. However, from Fig. 2c it is clearly observed that the CNT-COOH is uniformly distributed on the membrane surface.

Raman spectra of the unmodified PP membrane and CNIM-PP are depicted in Fig. 3a. Dominant Raman bands at 826, 865, 1003, 1124 cm^{-1} of PP backbone as observed in all spectra could be attributed to CH_2 wagging, twisting, symmetric and asymmetric stretch [33]. Intensity of the bands located at 973 $cm^{-1}$and 998 cm^{-1} was modified as a function of the angular position. The bands at 973 cm^{-1} and 998 cm^{-1} were assigned principally to the C-C asymmetric stretching mode of the skeletal backbones and to the rocking mode of the CH_3 lateral alkyl groups respectively. The upshift of Raman band at 1597 - 1603 cm^{-1} could be attributed to the carbonyl group in the D-band region and G-band region of CNTs [34]. Fig. 3.b shows the Confocal Raman Microscope Image of CNIM-PP membrane.

ACCEPTED MANUSCRIPT

The thermal stability of the CNIM-PP membrane was studied by thermogravimetric analysis (TGA). The TGA curves of plain and modified membranes are shown in Fig. 4. It is clear from the figure that the thermal stability of CNIM-PP membrane was enhanced due to the presence of CNTs.

3.2. DCMD performance of CNIM-PP membranes

The performance of CNIM-PP was evaluated and compared with unmodified PP membrane. The water vapor flux, J_w, across the membrane can be expressed as:

$$J_w = \frac{W_p}{t.A} \tag{5}$$

where, W_p is the total mass of permeate, t is the permeate collection time and A is the effective membrane surface area.

3.2.1. Effect of temperature and feed flow rate on water vapor flux

Fig. 5a shows the influence of temperature on water vapor flux of the CNIM-PP membranes compared to the unmodified PP membrane. It was observed that the permeate fluxes in all the membranes increased with temperature. The temperature increased the vapor pressure difference between feed and permeate side, hence the driving force for mass transport. As can be seen, the CNIMs exhibited higher water vapor flux compared to the unmodified PP. Flux was as high as 37.9 kg/m^2.hr at 70^{0}C for CNT-COOH-PP, which was 32.2% higher than that of unmodified PP.

In this work, we observed a higher overall water vapor flux in DCMD mode as compared to our previous work [28], probably due to the difference in feed flow rate (much higher in this case) and use of cold water in the permeate side that carry away the condensed water at a much

ACCEPTED MANUSCRIPT

faster rate than SGMD, resulting in higher mass transfer coefficient leading to higher permeate fluxes.

The effect of feed flow rate is shown in Fig. 5b. The feed flow rate during the experiment was varied between 100 – 320 mL/min. Permeate flow rate was kept constant around 250 mL/min for all the experiments. The figure clearly demonstrates the increase in water vapor flux with increase in feed velocity. The elevated flow rates increased turbulence and reduced the boundary layer which helped in lowering the temperature polarization and increased the driving force for MD.

3.3. Mass transfer coefficient:

Again, J_w can be denoted as:

$$J_w = k(P_f - P_p)$$

$$or, k = \frac{J_w}{(P_f - P_p)} \quad (2)$$

Where, k is the mass transfer coefficient, P_f and P_P is the partial water vapor pressure in feed and permeate side.

The overall mass transfer is controlled by diffusion through the boundary layer at low flow rates. It is well known that with increase in flow rate turbulence increases which in turn reduces the boundary layer at the membrane interface. It was observed from Fig. 6a that with increase in flow rate mass transfer coefficient increased significantly. The overall mass transfer coefficient was also increased slightly with increase in temperature as the rate of diffusion increased. This is shown in Fig. 6b. CNIM-PP membranes showed higher mass transfer coefficient compared to the unmodified PP membrane. Among the two CNIMs, CNT-COOH-PP

ACCEPTED MANUSCRIPT

exhibited higher mass transfer coefficient with an increment of 32.7 and 8.31% in comparison with unmodified PP and CNT-PP, respectively. The enhancement in mass transfer coefficient was observed much lower in comparison with our previously reported SGMD desalination configuration (an enhancement of 116% was observed). This may be due to the higher internal heat loss through the membrane in DCMD configuration [35].

3.4. Effect of salt concentration

Fig. 7a shows the influence of salt concentration in feed on water vapor flux. Higher salt concentrations lead to more temperature polarization which reduced the overall DCMD performances [36, 37]. Fouling and scaling with inorganic salt causes pore clogging in MD membranes which reduce the available membrane area for water vaporization and hence reduce the flux. In addition, scaling of the surfaces reduces the flow channel area which causes a pressure drop and lower flow rates, leading to higher temperature polarization effects and reduction in flux [38]. The brine also has slightly lower vapor pressure than pure water. Unmodified PP membrane shows a decrease in water vapor flux in the figure, as expected. However, the reduction of flux in CNIM-PP membranes is much less in comparison with unmodified PP. The presence of CNTs and pendent functional groups may increase the surface roughness and reduce the formation of boundary layers that allows higher driving force, hence flux.

Fig. 7b shows the effect of salt concentration on mass transfer coefficient of the membranes. All of the CNIM-PP membranes show higher mass transfer coefficient than unmodified PP membrane. The change in mass transfer coefficient values with increase in

ACCEPTED MANUSCRIPT

concentration is also very low for CNIM-PP membranes, whereas unmodified PP membrane shows a significant negative change with increased salt concentration.

3.5. Membrane stability and screening effect of CNTs

To study the stability of the membranes, DCMD was carried out for 60 days (8 hr per day) with 10000 ppm NaCl salt solution at 70^{o}C. The water vapor flux and salt concentration at permeate side was measured periodically. It was observed that there was no significant change in water vapor flux and salt rejection for the CNIM-PP. This is shown in Fig. 8. However, a slight decrease in flux (~6%) and salt rejection (~4%) was found for unmodified PP membrane after 6-7 days of operation and it required cleaning of the membrane to regain its original performances. This may be due to the fact that some salt may deposit on unmodified PP pores that reduces the overall flux and increase the salt concentration in the permeate. For CNIM-PP membranes, CNTs network may form an additional screen that resists direct deposition of salt over the membrane pores.

3.6. Proposed mechanism:

The CNIM-PP shows a significant enhancement in DCMD performance compared to the unmodified PP membrane. This could be attributed to the fact that the CNTs serves as sorbent sites for moisture transport while repelling the liquid water. The polar carboxylated functionalized CNTs offers higher sorption for the water moistures, thus improving overall flux. Further, enhanced hydrophobicity of the CNIM membrane also expected as PVDF was used as surface binder. The overall mechanism for functionalized CNTs is shown in Fig. 9a.

ACCEPTED MANUSCRIPT

The highly hydrophobic immobilized CNTs can act as folded membrane and increase the effective surface area for the generation of more water vapor as shown in the Fig. 9b and c. It also increases the linear velocity of the feed (as we observed that with increase in feed flow rate water vapor flux increased). Furthermore, the hindrance in flow may generate turbulence that also reduces the temperature polarization effect, hence the flux.

Among the CNIM-PP membranes, CNT-COOH-PP showed best performances followed by CNT-PP membrane. With functionalization of CNTs, the dispersibility of nanotubes enhanced that helps to fabricate a uniformly distributed CNIM. It is clear from SEM images that CNTCOOH offers better dispersion and uniform distribution over the PP support. Furthermore, the functional groups may act as a pendent over the CNT surfaces as shown in the Fig. 9d. It is important to note that the functional group contains a highly polar moiety that may serve as moisture sorbent site. The specific interactions of the water moisture with the functional groups are shown in the Fig. 9e.

4. Conclusions

We have synthesized functionalized CNTs immobilized membranes that alters the hydrophilic-hydrophobic interactions of the membrane surface with water moisture generated on the hydrophobic porous PP support from the hot feed solutions. The membranes were successfully employed to generate pure water from high concentration brine mixtures. The water flux achieved up to a maximum of 36.8 $kg/m^2.hr$ at 70^0C for CNT-COOH-PP membrane and salt reduction higher than 99.9%. For the same membrane, the mass transfer coefficient was found 1.5 times higher than that of unmodified PP membrane. The CNIM membranes showed stability over longer period of time without any fouling and breaking. The CNIM membrane also showed

ACCEPTED MANUSCRIPT

better thermal stability than unmodified PP membrane. These results encourage the incorporation of functionalized CNTs to provide an easy alternative of hydrophilic-hydrophobic DCMD membrane modification with enhanced flux and stability.

ACCEPTED MANUSCRIPT

ACCEPTED MANUSCRIPT

References:

[1] J. Zhang, N. Dow, M. Duke, E. Ostarcevic, J-D Li, S. Gray, Identification of material and physical features of membrane distillation membranes for high performance desalination, J. of Membr. Sci. 349 (2010), pp. 295-303

[2] M. Khayet, Membranes and theoretical modeling of membrane distillation: a review, Adv. Colloid Interface Sci., 164 (1-2) (2011), pp. 56–88

[3] M. Khayet, J.I. Mengual, T. Matsuura, Porous hydrophobic/hydrophilic composite membranes: application in desalination using direct contact membrane distillation, J. Membr. Sci., 252 (2005), pp. 101–113

[4] Z. Jin, D.L. Yang, S.H. Zhang, X.G. Jian, Hydrophobic modification of poly(phtalazinone ether sulfone ketone) hollow fiber membrane for vacuum membrane distillation, J. Membr. Sci., 310 (2008), pp. 20–27

[5] S.R. Krajewski, W. Kujawski, M. Bukowska, C. Picard, A. Larbot, Application of fluoroalkylsilanes (FAS) grafted ceramic membranes in membrane distillation process of NaCl solutions, J. Membr. Sci., 281 (2006), pp. 253–259

[6] M. Khayet, T. Matsuura, J.I. Mengual, Porous hydrophobic/hydrophilic composite membranes: estimation of the hydrophobic-layer thickness, J. Membr. Sci., 266 (2005), pp. 68–79

[7] M. Qtaishat, M. Khayet, T. Matsuura, Novel porous composite hydrophobic/hydrophilic polysulfone membranes for desalination by direct contact membrane distillation, J. Membr. Sci., 341 (2009), pp. 139–148

ACCEPTED MANUSCRIPT

[8] M. Bryjak, I. Gancarz, K. Smolinska, Plasma nanostructuring of porous membranes, Adv. Colloid Interface Sci., 161 (2010), pp. 2–9

[9] S. Bonyadi, T.S. Chung, Flux enhancement in membrane distillation by fabrication of dual layer hydrophilic–hydrophobic hollow fiber membranes, J. Membr. Sci., 306 (2007), pp. 134–146

[10] F. Edwie, T-S Chung, Development of hollow fiber membranes for water and salt recovery from highly concentrated brine via direct contact membrane distillation and crystallization, J. Membr. Sci., 421-422 (2012), pp. 111–123

[11] J.A. Prince, D. Rana, G. Singh, T. Matsuura, T. Jun Kai, T.S. Shanmugasundaram, Effect of hydrophobic surface modifying macromolecules on differently produced PVDF membranes for direct contact membrane distillation, Che. Engg. Journal, 242 (2014), pp. 387–396

[12] C. H. Cho, K.Y. Oh, S. K. Kim, J. G. Yeo, P. Sharma, Pervaporative seawater desalination using NaA zeolite membrane: Mechanisms of high water flux and high salt rejection, Jr. Membr. Sci. 371 (2011) 226-238.

[13] J.A. Prince, G. Singh, D. Rana, T. Matsuura, V. Anbharasi, T.S. Shanmugasundaram, Preparation and characterization of highly hydrophobic poly(vinylidene fluoride) – Clay nanocomposite nanofiber membranes (PVDF–clay NNMs) for desalination using direct contact membrane distillation, J. Membr. Sci., 397-398 (2012), pp. 80-86

[14] S. Khemakhem, R. B. Amar, Modification of Tunisian clay membrane surface by silane grafting: Application for desalination with Air Gap Membrane Distillation process, Colloids and Surfaces A: Physicochemical and Engineering Aspects, 387 (2011), pp. 79-85

ACCEPTED MANUSCRIPT

[15] H. Fang, J.F. Gao, H.T. Wang, C.S. Chen, Hydrophobic porous alumina hollow fiber for water desalination via membrane distillation process, J. Membr. Sci., 403-404 (2012), pp. 41-46

[16] Y. T. Ong, A. L. Ahmad, S. H. S. Zein, K. Sudesh, S. H. Tan, Poly(3-hydroxybutyrate)-functionalised multi-walled carbon nanotubes/chitosan green nanocomposite membranes and their application in Pervaporation, Sep. Purif. Techno.l 76 (2011), pp. 419-427

[17] Y. X. Jia, H. L. Li, M. Wang, L.Y. Wu, Y.D. Hu, Carbon nanotube: Possible candidate for forward osmosis, Sep. Purif. Technol.75 (2010), pp. 55-60

[18] S. Roy, S. A. Ntim, S. Mitra, K.K. Sirkar, Facile fabrication of superior nanofiltration membranes from interfacially polymerized CNT-polymer composites, J. Membr. Sci. 375 (2011), pp. 81-87

[19] V. Vatanpour, S. S. Madaeni, R. Moradian, S. Zinadini, B. Astinchap, Fabrication and characterization of novel antifouling nanofiltration membrane prepared from oxidized multiwalled carbon nanotube/polyethersulfone nanocomposites, J. Membr Sci. 375 (2011), pp. 284-294

[20] D. Manikandan, R. V. Mangalaraja, R. Siddheswaran, R. E. Avila, S. Ananthakumar, Fabrication of nanostructured clay–carbon nanotube hybrid nanofiller by chemical vapour deposition, Appl. Surf. Sci. 258 (2012), pp. 4460-4466

[21] A. Noy, H. G. Park, F. Fornasiero, J. K. Holt, C. P. Grigoropoulos, O. Bakajin, Nanofluidics in carbon nanotubes, Nano Today, 2 (2007), pp. 22-29

[22] R. Levenstein, D. Hasson, R. Semiat, Utilization of the Donnan effect for improving electrolyte separation with nanofiltration membranes, J. Membr. Sci. 116 (1996), pp. 77-92

ACCEPTED MANUSCRIPT

ACCEPTED MANUSCRIPT

[23] .V. Chung, N.Q. Buu, N.H. Chau, Influence of surface charge and solution pH on the performance characteristics of a nanofiltration membrane, Sci. Technol. Adv. Mater. 6 (2005), 246-250

[24] W. Mi, Y.S. Lin, Y. Li, Vertically aligned carbon nanotube membranes on macroporous alumina supports, J. Membr. Sci. 304 (2007), pp. 1-7

[25] L. F. Dumée, K. Sears, J. Schütz, N. Finn, C. Huynh, S. Hawkins, M. Duke, S. Gray, Characterization and evaluation of carbon nanotube Bucky-Paper membranes for direct contact membrane distillation, J. Membr. Sci. 351 (2010), pp. 36-43

[26] K. Gethard, O. S. Khow, S. Mitra, Water Desalination using Carbon-nanotube-enhanced Membrane Distillation, Appl. Mater. 3 (2011), pp. 110-114

[27] O. S. Khow, S. Mitra, Carbon Nanotube Immobilized Composite Hollow Fiber Membranes for Pervaporative Removal of Volatile Organics from Water, J. Phys. Chem. C 114 (2010), pp. 16351–16356

[28] M. Bhadra, S. Roy, S. Mitra, Enhanced desalination using carboxylated carbon nanotube immobilized membranes, Sep. and Purif. Technol, 120 (2013), pp. 373–377

[29] M. Khayet, C. Cojocaru, Artificial neural network model for desalination by sweeping gas membrane distillation, Desalination, Volume 308, 2 January 2013, Pages 102-110.

[30] M. Khayet, C. Cojocaru, A. Baroudi, Modeling and optimization of sweeping gas membrane distillation, Desalination,Volume 287, 15 February 2012, Pages 159–166.

ACCEPTED MANUSCRIPT

ACCEPTED MANUSCRIPT

[31] Y. Chen, Z. Iqbal, S. Mitra, Microwave-Induced Controlled Purification of Single-Walled Carbon Nanotubes without Sidewall Functionalization, Adv. Funct. Mater., 17 (2007), pp. 3946–3951.

[32] D. Wang, W.K. Teo, Preparation and characterization of polyvinylidene fluoride (PVDF) hollow fiber membranes, J. Membr. Sci., 163 (1999), pp. 211–220

[33] J.L. Koenig, Spectroscopy of Polymers, 2nd ed. Elsevier Sciences Inc., New York, 1999.

[34] Peter Larkin, Infrared and Raman Spectroscopy; Principles and Spectral Interpretation, Elsevier, USA, 2011.

[35] Mohamed Khayet Souhaimi, T. Matsuura, Membrane Distillation: Principles and Applications, Elsevier, The Netherlands, 2011.

[36] Y. Yun, R. Ma, W. Zhang, A. G. Fane, and J. Li, Direct contact membrane distillation mechanism for high concentration NaCl solutions, Desalination, 188 (2006), pp. 251–262

[37] L Martínez-Díez, M.I Vázquez-González, Temperature and concentration polarization in membrane distillation of aqueous salt solutions, J. Membr. Sci., 156 (1999), pp. 265–273

[38] A. Kullab and A. Martin, "Membrane distillation and applications for water purification in thermal cogeneration plants, Sep. and Purif. Technol, 76 (2011), pp. 231–237

ACCEPTED MANUSCRIPT

ACCEPTED MANUSCRIPT

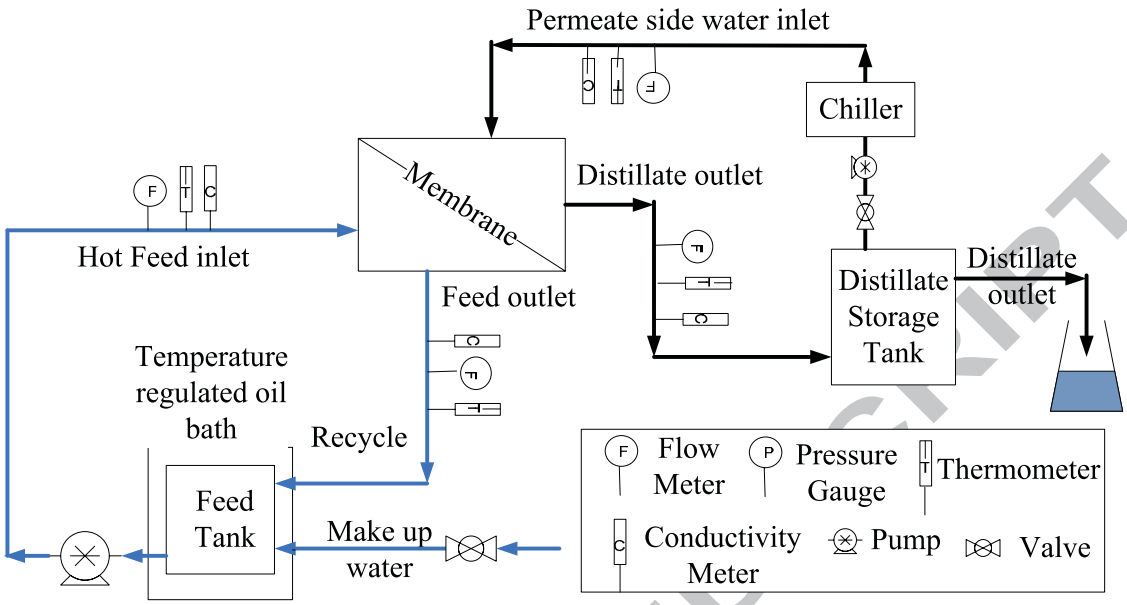

Fig. 1. Schematic diagram of the experimental set up for DCMD application

ACCEPTED MANUSCRIPT

ACCEPTED MANUSCRIPT

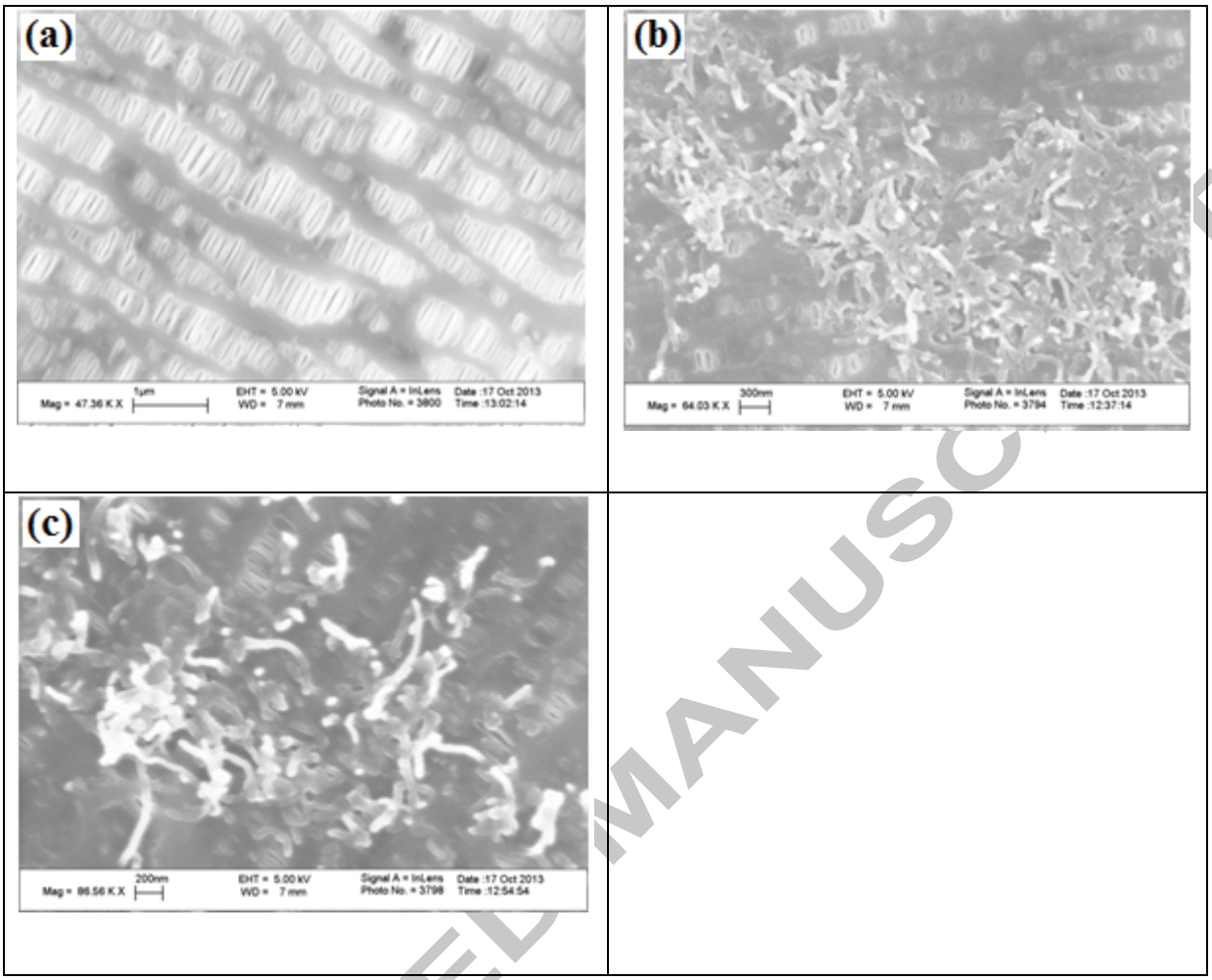

Fig. 2. SEM images of the surfaces of (a) PP membrane, (b) CNT-PP membrane and (c) CNT-COOH-PP membrane.

ACCEPTED MANUSCRIPT

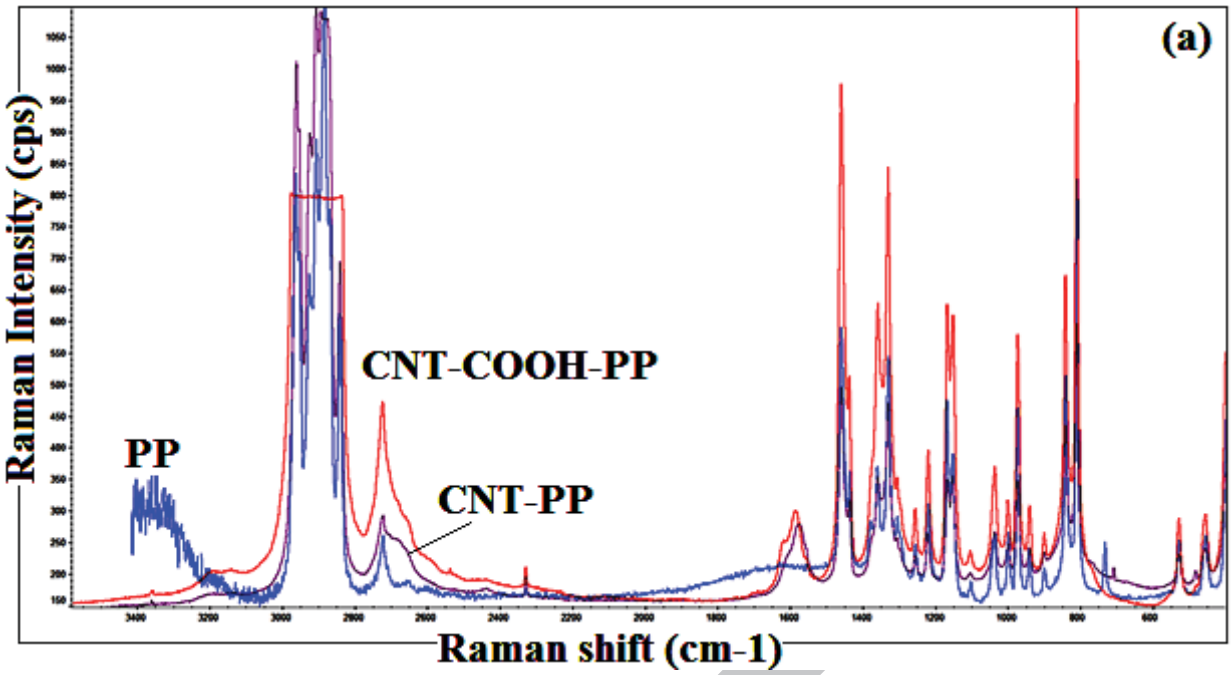

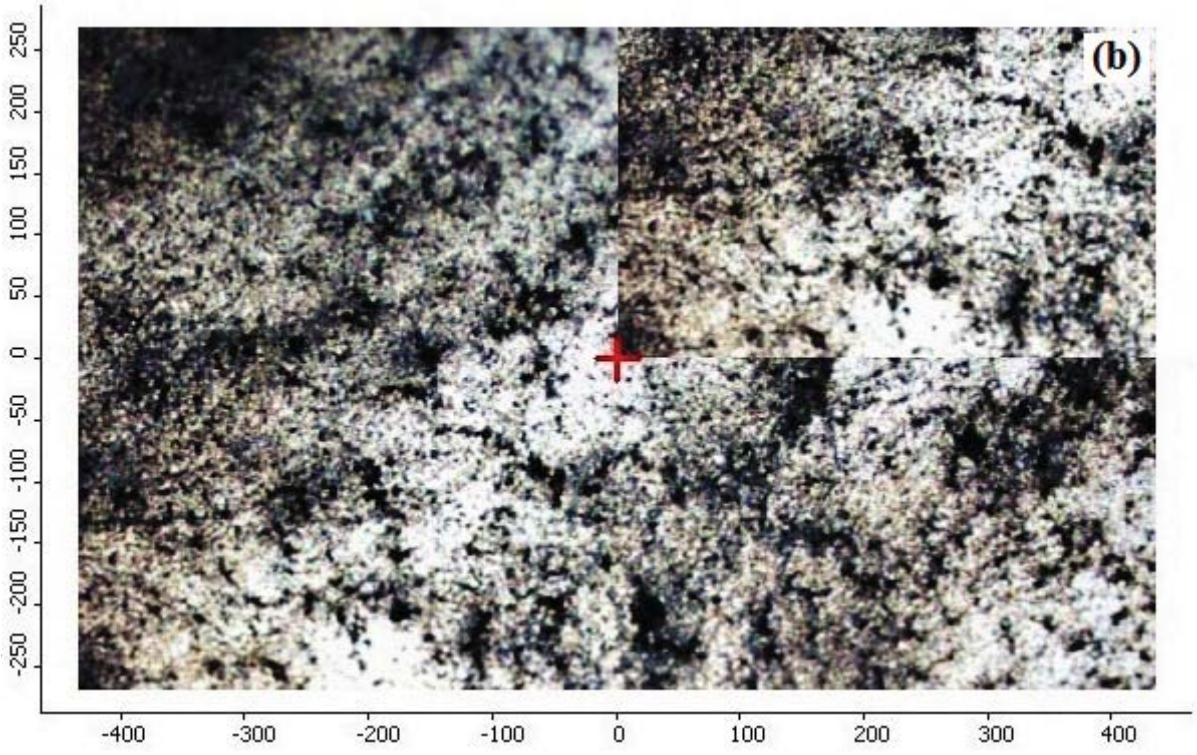

Fig. 3. (a) Raman spectra of PP, CNT-PP and CNT-COOH-PP, (b) Raman image of CNT-COOH-PP membrane.

ACCEPTED MANUSCRIPT

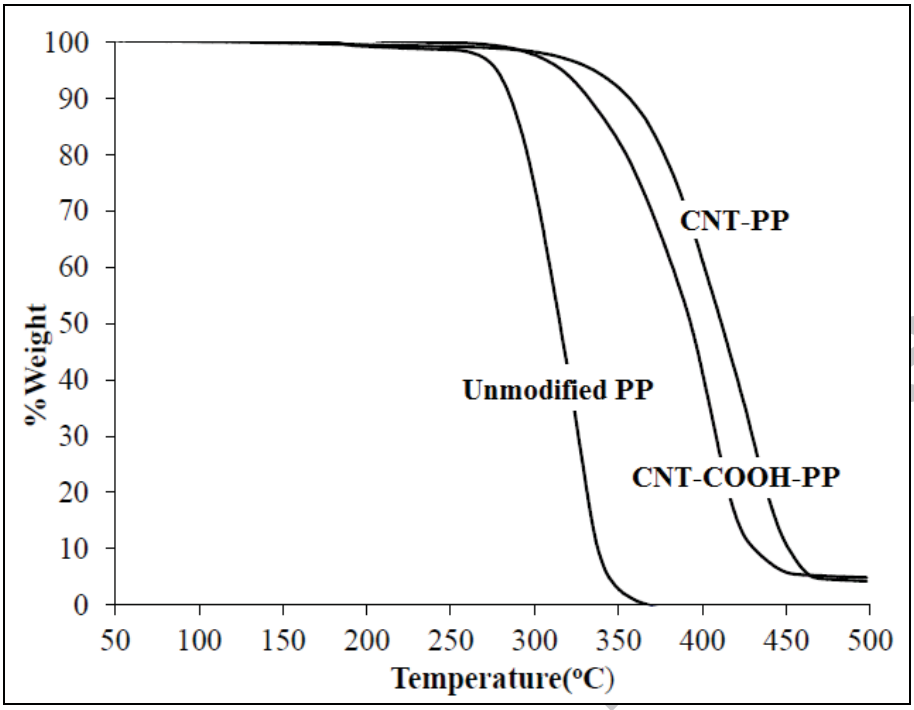

Fig. 4.TGA of PP, CNT-PP and CNT-COOH-PP

ACCEPTED MANUSCRIPT

ACCEPTED MANUSCRIPT

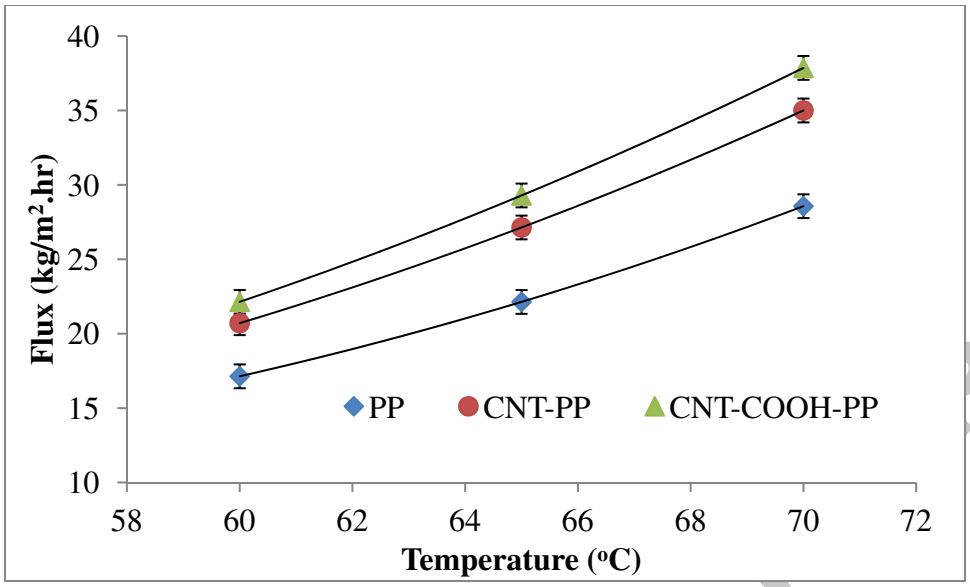

Fig. 5.a Effect of feed temperature on water vapor flux

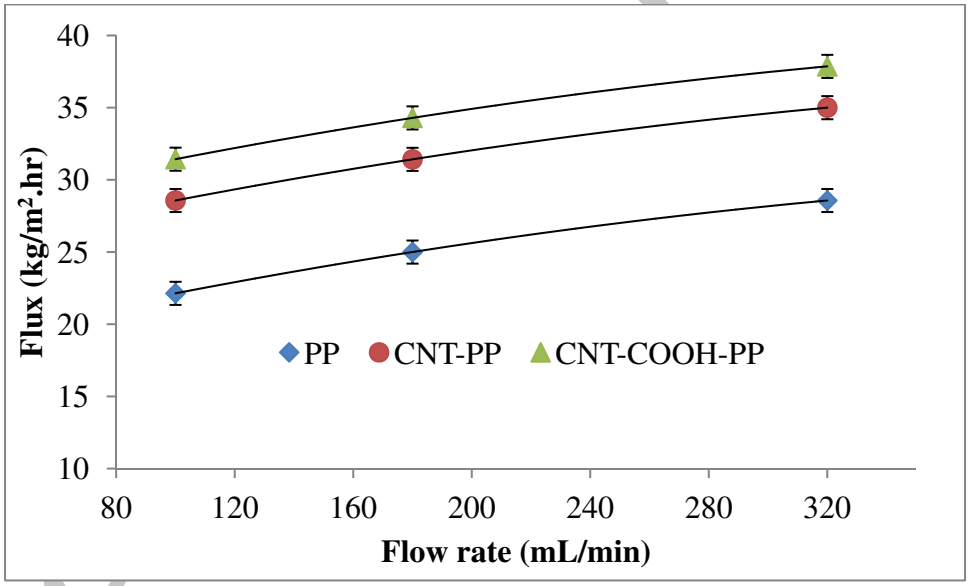

Fig. 5.b Effect of feed flow rate on water vapor flux

ACCEPTED MANUSCRIPT

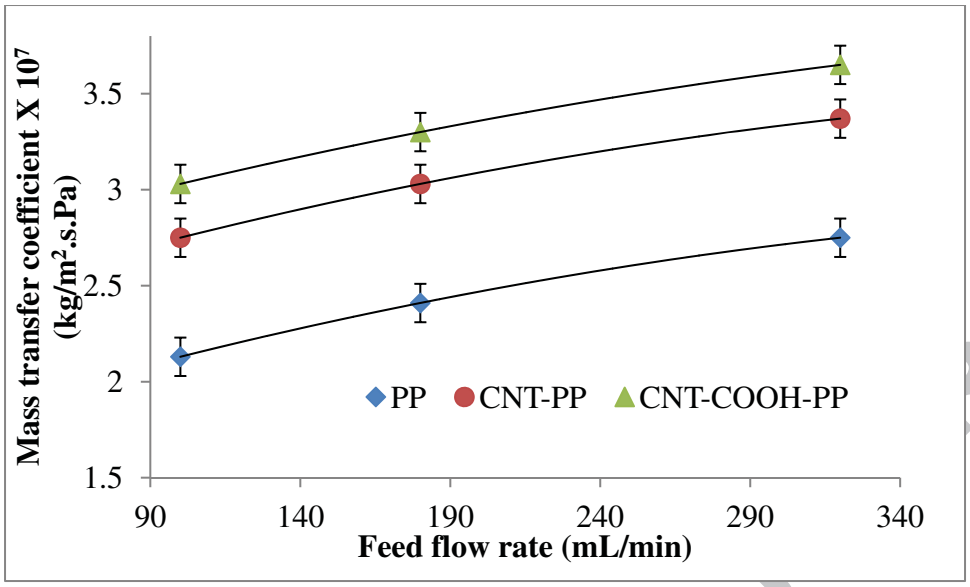

Fig. 6.a Effect of feed flow rate on mass transfer coefficient

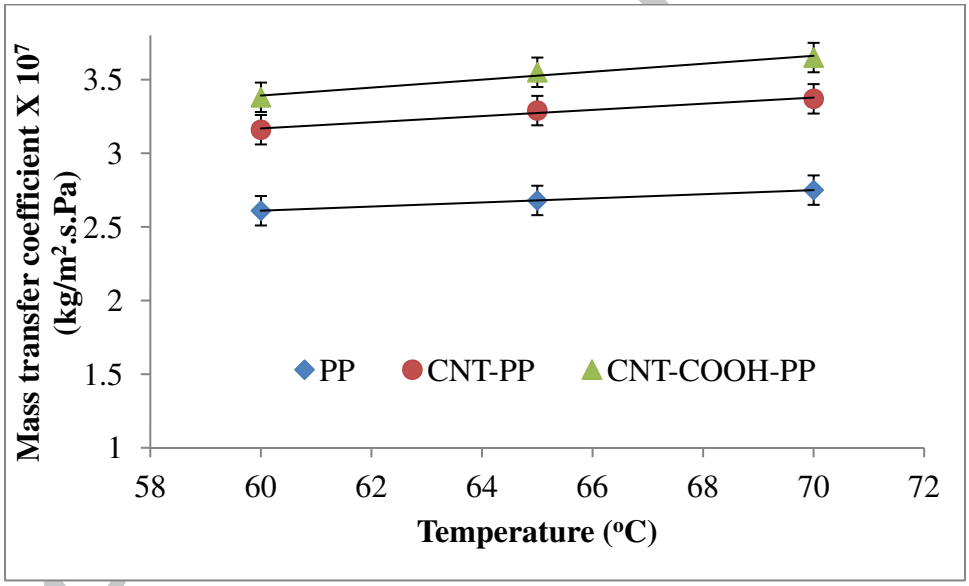

Fig. 6.b Effect of temperature on mass transfer coefficient

ACCEPTED MANUSCRIPT

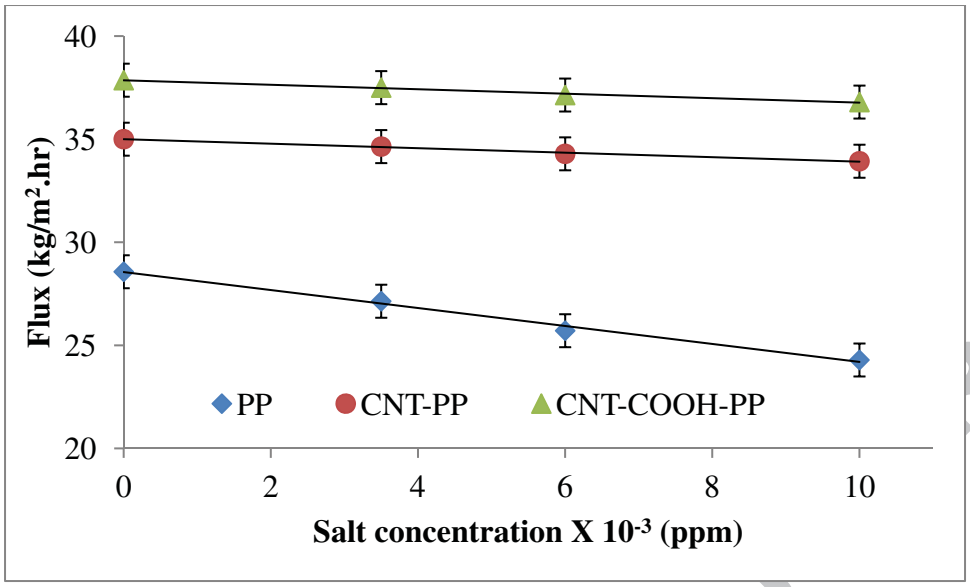

Fig. 7.a Effect of salt concentration in feed on water vapor flux

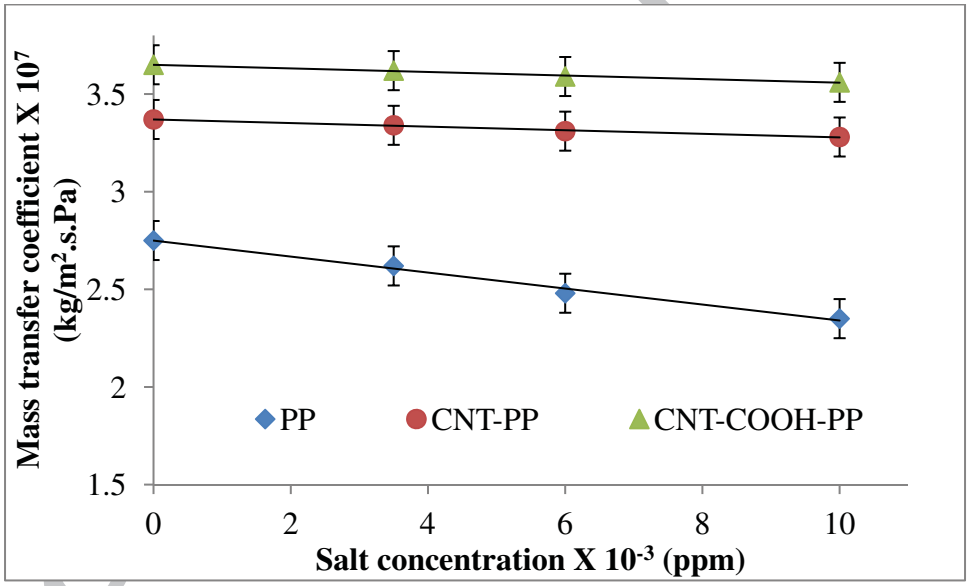

Fig. 7.b Effect of salt concentration in feed on mass transfer coefficient

ACCEPTED MANUSCRIPT

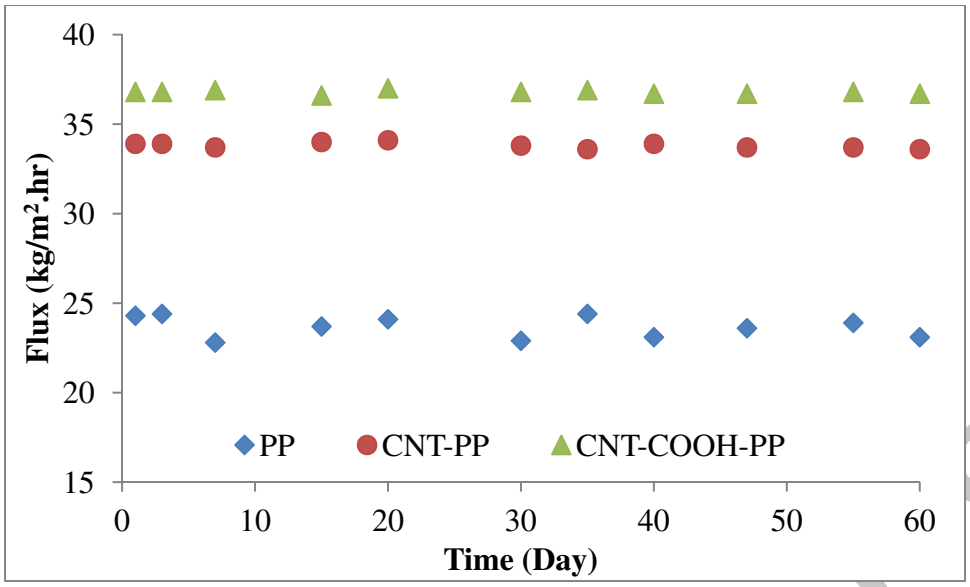

Fig. 8. Stability study of PP and CNIM-PP over an extended period

ACCEPTED MANUSCRIPT

ACCEPTED MANUSCRIPT

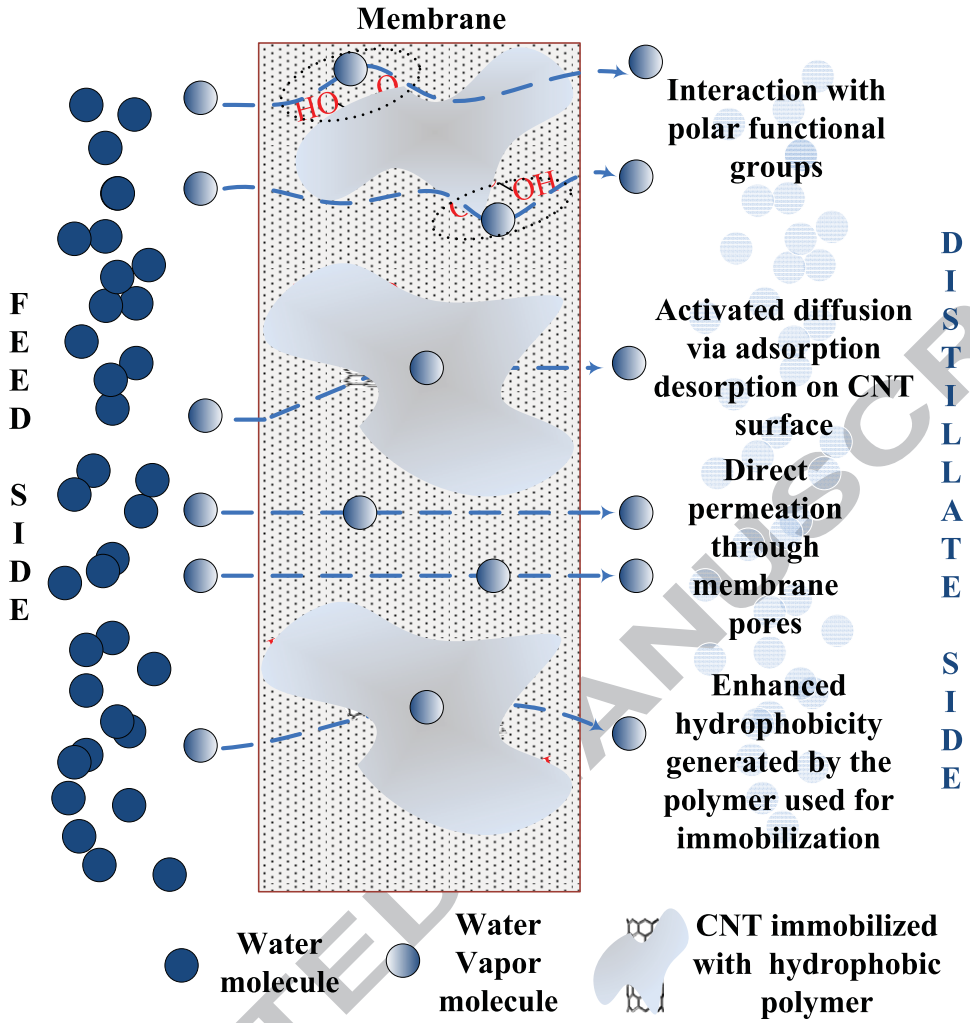

Fig. 9.a.Schematic of proposed mechanism for CNT-COOH-PP membrane

ACCEPTED MANUSCRIPT

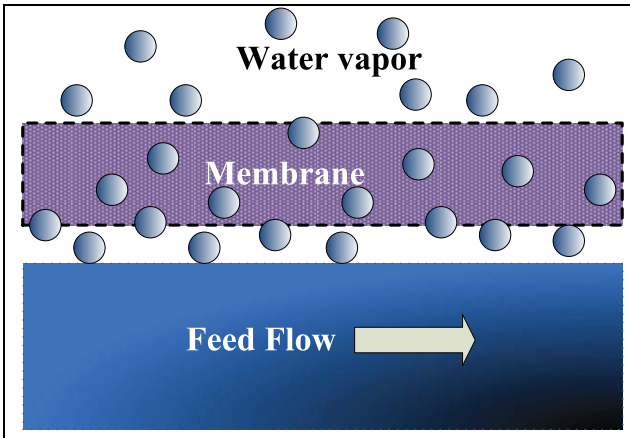

Fig. 9.b. Feed flow on a unmodified porous PP membrane

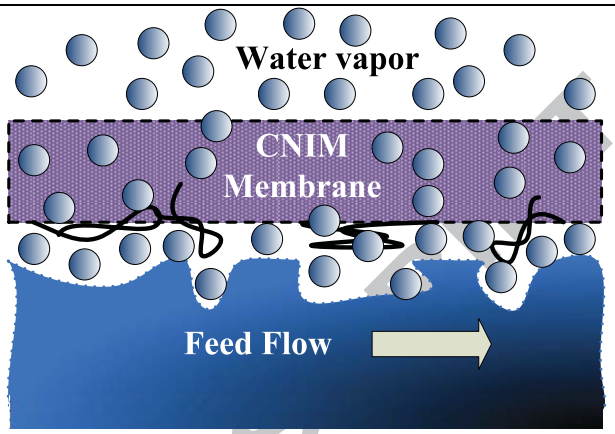

Fig. 9.c. Feed flow on a CNIM

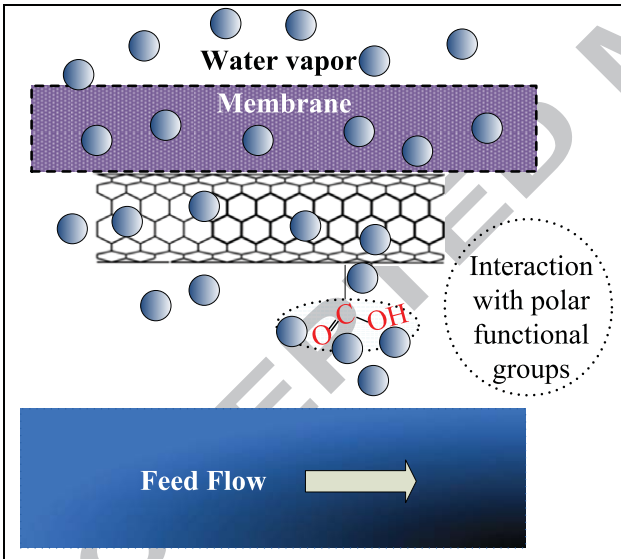

Fig. 9.d. Specific interaction of moisture with polar carboxylic acid (-COOH) on CNT-COOH-PP membrane

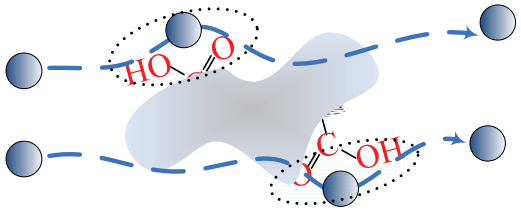

Fig. 9.e. Specific interaction of water moisture with polar carboxylic acid (-COOH) group of CNTs in CNT-COOH-PP membrane

ACCEPTED MANUSCRIPT

Highlights:

- Direct contact membrane distillation (DCMD) on carbon nanotube immobilized membranes (CNIM) is presented.
- Enhancement of water vapor flux was observed using functionalized CNTs.
- Mechanism of water vapor transport in DCMD in the presence of CNTs is presented.
- Higher salt concentration had negligible effect on the net water vapor flux in CNIM.

ACCEPTED MANUSCRIPT